

International Journal of Modern Physics D  
 © World Scientific Publishing Company

## DYNAMICAL SPATIAL CURVATURE AS A FIT TO TYPE IA SUPERNOVAE

CÉLIA DESGRANGE<sup>1</sup>, ASTA HEINESEN<sup>2</sup> AND THOMAS BUCHERT<sup>1</sup>

<sup>1</sup>*Univ Lyon, ENS de Lyon, Univ Lyon1, CNRS,  
 Centre de Recherche Astrophysique de Lyon UMR5574  
 Lyon, F-69007, France*

*Emails: celia.desgrange@ens-lyon.fr buchert@ens-lyon.fr*

<sup>2</sup>*School of Physical & Chemical Sciences, University of Canterbury, Private Bag 4800  
 Christchurch 8140, New Zealand*

*Email: asta.heinesen@pg.canterbury.ac.nz*

Received Day Month Year

Revised Day Month Year

Few statements in cosmology can be made without assuming a cosmological model within which to interpret data. Statements about cosmic acceleration is no exception to this rule, and the inferred positive volume acceleration of our Universe often quoted in the literature is valid in the context of the standard Friedmann-Lemaître-Robertson-Walker (FLRW) class of space-times.

Using the Joint Light-curve Analysis (JLA) catalogue of type Ia supernovae (SNIa), we examine the fit of a class of exact scaling solutions with dynamical spatial curvature formulated in the framework of a scalar averaging scheme for relativistic inhomogeneous space-times. In these models, global volume acceleration may emerge as a result of the non-local variance between expansion rates of clusters and voids, the latter gaining volume dominance in the late-epoch Universe.

We find best-fit parameters for a scaling model of backreaction that are reasonably consistent with previously found constraints from SNIa, CMB, and baryon acoustic oscillations data. The quality of fit of the scaling solutions is indistinguishable from that of the  $\Lambda$ CDM model and the timescape cosmology from an Akaike Information Criterion (AIC) perspective. This indicates that a broad class of models can account for the  $z < \sim 1$  expansion history.

*Keywords:* inhomogeneous universe model; backreaction; cosmological parameters; observational cosmology; supernovae type Ia

PACS numbers: 98.80.-k, 98.80.Es, 98.80.Jk, 95.36.+x

### 1. Introduction

Supernovae of type Ia, and their use as approximate standard candles, have led to one of the most remarkable observations made in cosmology: the volume growth of the Universe, when interpreted within the Friedmann-Lemaître-Robertson-Walker (FLRW) class of models, is accelerating.<sup>1-3</sup>

2 CÉLIA DESGRANGE, ASTA HEINESEN AND THOMAS BUCHERT

This discovery, together with BAO (baryon acoustic oscillations) features in the galaxy distribution and the CMB (cosmic microwave background), serves as a further observational cornerstone of the  $\Lambda$ CDM paradigm (cold dark matter with dark energy modeled by a positive cosmological constant  $\Lambda$ ) as the most successful expansion history within the FLRW class of models. The largely self-consistent fit of the  $\Lambda$ CDM model to data comes at the expense of introducing unknown energy-momentum sources. There are also a number of observational tensions;<sup>4–11</sup> for a recent overview see Ref. 12.

Given these mysteries encountered when interpreting cosmological data in the FLRW models, it might be worth to reconsider their status as being the almost exclusively studied solutions of the Einstein equations in cosmology. The FLRW metrics offer a simple framework within which to interpret observations, but are extremely limited in their dynamical features. The extent to which the standard FLRW models can accurately serve as a global ‘background’ and provide an average description for the all-scale hierarchy of structures in the Universe must be assessed.

The real Universe is not spatially homogeneous and isotropic, but is at best associated with *statistical* symmetries on ‘cosmological scales’. Whether a statistical description properly marginalizing over the hierarchy of structures in our Universe will yield an FLRW space-time as an accurate description of large-scale cosmic dynamics is not evident from first principles.

In our analysis we employ a covariant scalar averaging scheme<sup>13,14</sup> appropriate for marginalizing over structure in a general relativistic cosmological fluid description to obtain global evolution equations analogous to Friedmann’s equations for space-times with no imposed symmetries. One of the main insights of this scalar averaging scheme is that average spatial curvature is gravitationally unstable:<sup>15</sup> maintaining (close to) zero global spatial curvature (which is a built in feature of the  $\Lambda$ CDM paradigm of cosmology) in a general relativistic universe model with structure requires fine-tuning at all stages of the expansion history. In the averaging scheme which we employ, the FLRW spatial curvature behaviour does not follow naturally as an averaged description in universe models without assuming *exact* spatial homogeneity and isotropy. In particular, the flat  $\Lambda$ CDM model constrains spatial curvature to remain zero for all times, a property which is in general not recovered when averaging a lumpy space-time.

In this paper we consider a class of ‘scaling solutions’,<sup>15–17</sup> which forms a closure condition for the system of general cosmological equations for averaged scalar variables. These solutions have average spatial curvature evolution which is fundamentally different from that of the FLRW class of space-times. Some observational tests have already been made with these scaling solutions in Ref. 17, using CMB data and a sparse SNIa sample, and in Ref. 18, using BAO measurements and the differential age method.

Another model built from the same scalar averaging scheme as the scaling so-

lutions, the ‘timescape model’,<sup>a</sup> has been tested on the Joint Light-curve Analysis (JLA)<sup>20</sup> catalogue of type Ia supernovae and showed an equally good fit to that of the spatially flat  $\Lambda$ CDM model. The successful fit of the timescape model suggests that spatial curvature evolution has the potential of mimicking dark energy in the late epoch Universe. Curvature evolution in the late epoch Universe has first been applied to supernova data by Kasai<sup>22</sup> by dividing the supernova sample into early- and late-type subsamples and fitting these two subsamples with different FLRW models, treating the respective FLRW curvature parameters as free parameters in the analysis. While it is known that the FLRW model with negative constant curvature does not successfully fit cosmological data, nothing in this result prevents non-FLRW curvature evolution towards present-epoch negative curvature—as expected from general considerations of averaged inhomogeneous universe models.<sup>21</sup>

In this work we use the JLA catalogue to test a family of scaling solutions for the average variables entering in the scalar averaging scheme using the Spectral Adaptive Lightcurve Template 2 (SALT2) relation. We will compare the resulting fit to that of the  $\Lambda$ CDM model, the empty universe model,<sup>b</sup> and the timescape model.

In Sec. 2 we review the scalar averaging scheme and the scaling solutions employed in this paper, and we provide the distance modulus–redshift relation for the scaling solutions. In Sec. 3 we briefly describe the SALT2 method for standardising supernovae, and we review the likelihood-function used in the statistical analysis of the JLA catalogue. In Sec. 4 we present the results of our analysis: constraints on model parameters of the investigated scaling solutions, and the quality of fit as compared to that of the  $\Lambda$ CDM model, the empty Milne model (i.e. the FLRW model without sources, but negative constant curvature), and the timescape model. In Sec. 5 we examine a FLRW curvature consistency measure, compute the analogous measure for the best-fit results for the scaling solutions, and discuss the potential use of this measure for the discrimination between FLRW models and backreaction models with emerging deviations from the FLRW constant curvature geometry in future surveys. We conclude in Sec. 6.

## 2. The scalar averaging scheme and scaling solutions

We now recall the class of scaling solutions of the scalar averaging scheme and provide an associated distance modulus–redshift relation, which we are going to test in this paper.

We base our analysis on a scheme for averaging of scalar variables in a self-gravitating dust-fluid, recalled in Sec. 2.1, and formulated in terms of effective cosmological parameters in Sec. 2.2. In Sec. 2.3 we introduce the scaling solutions,

<sup>a</sup>For a review of the timescape model see Ref. 19.

<sup>b</sup>While the empty universe model is unphysical and ruled out by combined constraints from CMB, SNIa, and BAO data, it is an interesting idealization for the *late-epoch Universe* in which matter is highly clustered within tiny volumes and photons primarily propagate in large, empty void-regions.

and in Sec. 2.4 we describe our procedure for constructing an effective metric, a so-called template metric, to match an effective light cone structure to the large-scale model defined in the averaging scheme. From this prescribed metric we finally obtain the expressions for the distance modulus–redshift relation in Sec. 2.5.

### 2.1. Irrotational dust averages

We consider a Lorentzian manifold with a self-gravitating irrotational dust fluid as the energy-momentum source in the Einstein equations. The aim is to describe average dynamical properties of this system, and to determine an effective description of light propagation on cosmological scales without knowing the metric of the lumpy space-time in detail.

The exact scalar averaging scheme we employ is a method for obtaining global dynamical equations for such a space-time, without knowledge of its ‘micro state’. Here we provide the relevant dynamical equations for this analysis with a short explanation of the relevant variables. Precise definitions of the variables and the averaging operation, and the full derivation of the below equations can be found in Ref. 13. Throughout this paper we work in units of  $c = 1$ ,  $c$  being the speed of light in vacuum.

Let  $\mathbf{u} = -\nabla t$  be the 4-velocity field of the fluid source, with  $t$  being a proper time function of the fluid, and let  $\varrho$  be its rest mass density. From averaging the local Raychaudhuri equation in the fluid rest frame over a spatial domain  $\mathcal{D}$  comoving with the fluid (no net-flux of particle world-lines through the boundaries of the averaging domain), we obtain the *averaged Raychaudhuri equation*,

$$3 \frac{\ddot{a}_{\mathcal{D}}}{a_{\mathcal{D}}} + 4\pi G \langle \varrho \rangle_{\mathcal{D}} - \Lambda = \mathcal{Q}_{\mathcal{D}}, \quad (1)$$

where  $a_{\mathcal{D}}$  is the volume scale factor,  $\langle \cdot \rangle_{\mathcal{D}}$  denotes averaging in the fluid frame over the comoving spatial domain  $\mathcal{D}$ ,  $\Lambda$  is the cosmological constant,<sup>c</sup> and the overdot denotes covariant time-derivative.  $\mathcal{Q}_{\mathcal{D}}$  is the ‘kinematical backreaction’ which is defined from the variance of the rate of expansion of the fluid congruence and the averaged shear of the fluid congruence over the domain  $\mathcal{D}$ .

The local energy constraint equation can be averaged in a similar way to obtain the averaged energy constraint equation,

$$3 \left( \frac{\dot{a}_{\mathcal{D}}}{a_{\mathcal{D}}} \right)^2 - 8\pi G \langle \varrho \rangle_{\mathcal{D}} - \Lambda = - \frac{\langle \mathcal{R} \rangle_{\mathcal{D}} + \mathcal{Q}_{\mathcal{D}}}{2}, \quad (2)$$

where  $\langle \mathcal{R} \rangle_{\mathcal{D}}$  is the averaged spatial scalar curvature. Finally, we have the average of the local energy-momentum conservation equation,

$$\langle \varrho \rangle_{\mathcal{D}} \dot{\phantom{\varrho}} + 3 \frac{\dot{a}_{\mathcal{D}}}{a_{\mathcal{D}}} \langle \varrho \rangle_{\mathcal{D}} = 0. \quad (3)$$

<sup>c</sup>We set  $\Lambda = 0$  in the investigations of this paper, as we investigate averaged models without dark energy, but keep  $\Lambda$  in the equations of this section for completeness.

All of the global variables  $a_{\mathcal{D}}$ ,  $\langle \varrho \rangle_{\mathcal{D}}$ ,  $\mathcal{Q}_{\mathcal{D}}$ , and  $\langle \mathcal{R} \rangle_{\mathcal{D}}$  entering in the averaged equations depend on the proper time slice parameterized by  $t$  and the spatial domain of integration  $\mathcal{D}$ .

Note that when positive,  $\mathcal{Q}_{\mathcal{D}}$  can act as an effective source for global acceleration in (1).  $\mathcal{Q}_{\mathcal{D}}$  will in general depend on cosmic time  $t$ , and on spatial scale through the dependence on the domain of averaging.

Combining (1), (2), and (3), the variables have to obey the following *integrability condition*:

$$\frac{1}{a_{\mathcal{D}}^6} (\mathcal{Q}_{\mathcal{D}} a_{\mathcal{D}}^6)^\cdot + \frac{1}{a_{\mathcal{D}}^2} (\langle \mathcal{R} \rangle_{\mathcal{D}} a_{\mathcal{D}}^2)^\cdot = 0, \quad (4)$$

Eq. (4) shows that kinematical backreaction and the averaged spatial curvature are coupled. This equation is key to understanding the evolution of global curvature as a consequence of structure formation. Note that by demanding  $\mathcal{Q}_{\mathcal{D}} \propto 1/a_{\mathcal{D}}^6$  (including the trivial case  $\mathcal{Q}_{\mathcal{D}} = 0$ ), the averaged curvature obeys a separate (scale-dependent) conservation equation corresponding to the FLRW curvature constraint  $(\langle \mathcal{R} \rangle_{\mathcal{D}} a_{\mathcal{D}}^2)^\cdot = 0$ .

## 2.2. Cosmological parameters

It shall be convenient to write the averaged energy constraint equation (2) in terms of effective cosmological parameters.<sup>23</sup> Dividing (2) by  $(3H_{\mathcal{D}}^2)$ , where we call the functional  $H_{\mathcal{D}} \equiv \dot{a}_{\mathcal{D}}/a_{\mathcal{D}}$  ‘the global Hubble parameter’, we have:

$$\Omega_m^{\mathcal{D}} + \Omega_{\Lambda}^{\mathcal{D}} + \Omega_{\mathcal{R}}^{\mathcal{D}} + \Omega_{\mathcal{Q}}^{\mathcal{D}} = 1, \quad (5)$$

where the four cosmological ‘parameters’  $\Omega_m^{\mathcal{D}}$ ,  $\Omega_{\Lambda}^{\mathcal{D}}$ ,  $\Omega_{\mathcal{R}}^{\mathcal{D}}$ , and  $\Omega_{\mathcal{Q}}^{\mathcal{D}}$  constitute the ‘cosmic quartet’ and are defined by:

$$\Omega_m^{\mathcal{D}} \equiv \frac{8\pi G}{3H_{\mathcal{D}}^2} \langle \varrho \rangle_{\mathcal{D}}; \quad \Omega_{\Lambda}^{\mathcal{D}} \equiv \frac{\Lambda}{3H_{\mathcal{D}}^2}; \quad (6)$$

$$\Omega_{\mathcal{R}}^{\mathcal{D}} \equiv -\frac{\langle \mathcal{R} \rangle_{\mathcal{D}}}{6H_{\mathcal{D}}^2}; \quad \Omega_{\mathcal{Q}}^{\mathcal{D}} \equiv -\frac{\mathcal{Q}_{\mathcal{D}}}{6H_{\mathcal{D}}^2}. \quad (7)$$

As we wish to see whether the averaged spatial curvature  $\Omega_{\mathcal{R}}^{\mathcal{D}}$  and backreaction  $\Omega_{\mathcal{Q}}^{\mathcal{D}}$  cosmological parameters can mimic dark energy without a local energy component violating the strong energy condition, we set  $\Omega_{\Lambda}^{\mathcal{D}} = 0$ . We can further rewrite (5) in terms of deviations from a spatially flat Friedmannian parametrization,

$$\Omega_m^{\mathcal{D}} + \Omega_{\mathcal{X}}^{\mathcal{D}} = 1; \quad \Omega_{\mathcal{X}}^{\mathcal{D}} \equiv \Omega_{\mathcal{R}}^{\mathcal{D}} + \Omega_{\mathcal{Q}}^{\mathcal{D}}, \quad (8)$$

where  $\mathcal{X}$  stands for ‘ $\mathcal{X}$ -matter’: an effective ‘matter’ cosmological component that has the potential to mimic dark energy and/or dark matter signatures as they appear in the standard  $\Lambda$ CDM model.

### 2.3. Scaling solutions to the averaged Einstein equations

In order to uniquely determine the solutions to the four unknown functions  $a_{\mathcal{D}}$ ,  $\langle \varrho \rangle_{\mathcal{D}}$ ,  $\langle \mathcal{R} \rangle_{\mathcal{D}}$ , and  $\mathcal{Q}_{\mathcal{D}}$  satisfying the equations (1)–(4) (where one of the equations in the set is redundant), we must specify one additional equation as a closure condition.

We shall consider space-times which are consistent with the exact scaling solutions for the averaged spatial curvature and kinematical backreaction variables as formulated in Ref. 16, 17,

$$\langle \mathcal{R} \rangle_{\mathcal{D}} = \langle \mathcal{R} \rangle_{\mathcal{D}_i} a_{\mathcal{D}}^n ; \quad \mathcal{Q}_{\mathcal{D}} = \mathcal{Q}_{\mathcal{D}_i} a_{\mathcal{D}}^p , \quad (9)$$

as an ansatz for the needed closure condition, with  $n$  and  $p$  being real numbers, and  $\mathcal{D}_i$  denoting an initial domain for which the definition  $a_{\mathcal{D}_i} \equiv 1$  is imposed. Plugging the ansatz (9) into the integrability condition (4) we have that either  $n = -2$  and  $p = -6$  or  $n = p$  must be satisfied.

The solution  $n = -2$  and  $p = -6$  leads to a quasi-Friedmannian model in which the backreaction variable  $\mathcal{Q}_{\mathcal{D}}$  is negligible today (due to its rapid fall-off as a function of volume), and which is the only case where structure formation, encoded in  $\mathcal{Q}_{\mathcal{D}}$ , is decoupled from the averaged spatial curvature, such that the quasi-FLRW curvature constraint  $(\langle \mathcal{R} \rangle_{\mathcal{D}} a_{\mathcal{D}}^2) \cdot = 0$  is satisfied.

In the present analysis we will consider the class of solutions  $n = p$ , which imply coupling of structure formation and averaged scalar curvature. For this class of solutions we have the proportionality relation

$$\mathcal{Q}_{\mathcal{D}} = -\frac{n+2}{n+6} \langle \mathcal{R} \rangle_{\mathcal{D}} \quad (10)$$

between kinematical backreaction and averaged spatial curvature. Thus, positive kinematical backreaction (dominance of the variance in the fluid expansion rate over shear<sup>13</sup>) implies negative spatial curvature when  $n > -2$ .

It is convenient to introduce the following effective deceleration parameter for characterizing the different possible scaling solutions in terms of their acceleration:<sup>d</sup>

$$q_{\mathcal{D}} \equiv -\frac{\ddot{a}_{\mathcal{D}} a_{\mathcal{D}}}{\dot{a}_{\mathcal{D}}^2} = \frac{\Omega_m^{\mathcal{D}} - (n+2)\Omega_{\mathcal{X}}^{\mathcal{D}}}{2} = \frac{\Omega_m^{\mathcal{D}_0} - (n+2)\Omega_{\mathcal{X}}^{\mathcal{D}_0} \left(\frac{a_{\mathcal{D}}}{a_{\mathcal{D}_0}}\right)^{n+3}}{2\Omega_m^{\mathcal{D}_0} + 2\Omega_{\mathcal{X}}^{\mathcal{D}_0} \left(\frac{a_{\mathcal{D}}}{a_{\mathcal{D}_0}}\right)^{n+3}}, \quad (11)$$

analogous to the definition of the FLRW deceleration parameter. The second equality follows from combining (1) and (2), and using the definitions of the cosmological parameters given in Sec. 2.2. The last equality follows from the scaling conditions (9) with  $n = p$ , and from (8). From (11), we can formulate the following acceleration condition:

$$q_{\mathcal{D}} < 0 \quad \Leftrightarrow \quad (n+2) \left(\frac{a_{\mathcal{D}}}{a_{\mathcal{D}_0}}\right)^{n+3} > \frac{\Omega_m^{\mathcal{D}_0}}{1 - \Omega_m^{\mathcal{D}_0}}, \quad (12)$$

<sup>d</sup>Parameters evaluated at the present epoch are indexed with  $\mathcal{D}_0$  throughout this paper.

valid for  $0 < \Omega_m^{\mathcal{D}_0} < 1$ . Thus, for  $n \leq -2$ , volume acceleration does not occur at any epoch, as the kinematical backreaction  $Q_{\mathcal{D}}$  is negative in this case. For  $n > -2$ , acceleration might be reached depending on the value of  $\Omega_m^{\mathcal{D}_0}$ . We note that  $n = 0$  results in an acceleration condition formally similar to the flat FLRW model ( $\Omega_\Lambda = 1 - \Omega_m$ ) acceleration condition:  $2(a/a_0)^3 > \Omega_{m_0}/(1 - \Omega_{m_0})$ , where  $a$  is the FLRW scale factor. This is expected, since the backreaction term  $Q_{\mathcal{D}}$  is constant in this case, and thus acts as an effective cosmological constant in the averaged Raychaudhuri equation (1) (*cf.* Ref. 23 [Sec. 3.3.2]).

#### 2.4. The template metric

In order to translate physical observables of redshift and photon flux into ‘measurements’ of the free parameters  $n$  and  $\Omega_m^{\mathcal{D}_0}$  of the scaling solutions outlined in Sec. 2.3, we must parameterize predictions of the observables in terms of  $n$  and  $\Omega_m^{\mathcal{D}_0}$ .

We introduce a metric template as a constant-curvature metric but which, unlike the FLRW solution, allows for curvature evolution in ‘cosmic time’. The form of the effective metric follows the proposal of Ref. 17:

$${}^4g^{\mathcal{D}} \equiv -dt^2 + L_{H_{\mathcal{D}_0}}^2 a_{\mathcal{D}}^2 \left( \frac{dr_{\mathcal{D}}^2}{1 - \kappa_{\mathcal{D}}(t)r_{\mathcal{D}}^2} + r_{\mathcal{D}}^2 d\Omega^2 \right), \quad (13)$$

with  $t$  being the proper time function of the dust fluid, such that  $t = \text{const.}$  selects hypersurfaces orthogonal to the fluid flow, and  $r_{\mathcal{D}}$  is a dimensionless radial coordinate, which also has the interpretation as a comoving distance;  $a_{\mathcal{D}}$  is the dimensionless volume scale factor governed by (1)–(4), and  $a_{\mathcal{D}_0} L_{H_{\mathcal{D}_0}} \equiv H_{\mathcal{D}_0}^{-1}$  is the present-day Hubble horizon;  $d\Omega^2 \equiv (d\theta^2 + \sin(\theta)^2 d\phi^2)$  is the angular element on the unit sphere, and  $\kappa_{\mathcal{D}}$  is a dimensionless spatial constant-curvature function related to the averaged spatial Ricci scalar through

$$\kappa_{\mathcal{D}}(t) \equiv \frac{\langle \mathcal{R} \rangle_{\mathcal{D}}(t) a_{\mathcal{D}}^2(t)}{|\langle \mathcal{R} \rangle_{\mathcal{D}_0}| a_{\mathcal{D}_0}^2}. \quad (14)$$

For the class of scaling solutions described in Sec. 2.3, with  $n = p$ , one can rewrite  $\kappa_{\mathcal{D}}$  using (8) and (10):

$$\kappa_{\mathcal{D}}(a_{\mathcal{D}}) = - \frac{(n+6)\Omega_{\mathcal{X}}^{\mathcal{D}_0} a_{\mathcal{D}}^{(n+2)}}{|(n+6)\Omega_{\mathcal{X}}^{\mathcal{D}_0}| a_{\mathcal{D}_0}^{(n+2)}}. \quad (15)$$

In what follows we advance the idealizing conjecture that light propagation over cosmological scales is effectively described by null geodesics in the template metric (13). This is an assumption that follows the homogeneous-geometry approximation of the standard model, but corrects for the evolution of curvature to comply with the exact average properties. We note that the template metric is effective and not a solution of Einstein’s equations (for corresponding solutions see the recent paper by Stichel<sup>24</sup> and references therein). We also note that more insight and work is needed to improve on this first-step template metric.

### 2.5. Distance modulus

In order to constrain the scaling solutions with supernova data we must make a prediction for the distance modulus within this class of models. We will compute the distance modulus as a function of redshift in the template metric of Sec. 2.4.

The distance modulus is defined in terms of the luminosity distance  $d_L$  in the following way:

$$\mu(z_{\mathcal{D}}) = 5 \log_{10} \left( \frac{d_L(z_{\mathcal{D}})}{10 \text{ Mpc}} \right), \quad (16)$$

where  $z_{\mathcal{D}}$  is the redshift as inferred from the domain-dependent scale factor (see the below equation (19)). By Etherington's theorem (see Ref. 25 and references therein),

$$d_L(z_{\mathcal{D}}) = (1 + z_{\mathcal{D}})^2 d_A(z_{\mathcal{D}}), \quad (17)$$

where  $d_A$  is the angular diameter distance. The angular diameter distance is given via the metric (13) as

$$d_A(z_{\mathcal{D}}) = \frac{1}{H_{\mathcal{D}_0}} a_{\mathcal{D}}(z_{\mathcal{D}}) r_{\mathcal{D}}(z_{\mathcal{D}}). \quad (18)$$

From the geodesic equation of (13) we have that light emitted and absorbed by observers comoving with the dust, and propagating radially with respect to the central observer, is redshifted by<sup>e</sup>

$$z_{\mathcal{D}}(a_{\mathcal{D}}) = \frac{\hat{k}^0(a_{\mathcal{D}})}{a_{\mathcal{D}}} - 1, \quad (19)$$

with  $\hat{k}^0$  given by

$$\frac{d \ln(\hat{k}^0)}{da_{\mathcal{D}}} = - \frac{r_{\mathcal{D}}^2(a_{\mathcal{D}})}{2(1 - \kappa_{\mathcal{D}}(a_{\mathcal{D}})r_{\mathcal{D}}^2(a_{\mathcal{D}}))} \frac{d\kappa_{\mathcal{D}}(a_{\mathcal{D}})}{da_{\mathcal{D}}}. \quad (20)$$

The dimensionless coordinate distance  $r_{\mathcal{D}}$  along the null rays is

$$\frac{dr_{\mathcal{D}}}{da_{\mathcal{D}}} = - \frac{1}{a_{\mathcal{D}}^2} \sqrt{\frac{1 - \kappa_{\mathcal{D}}(a_{\mathcal{D}})r_{\mathcal{D}}^2(a_{\mathcal{D}})}{\Omega_m^{\mathcal{D}_0} a_{\mathcal{D}}^{-3} + \Omega_{\mathcal{X}}^{\mathcal{D}_0} a_{\mathcal{D}}^n}}, \quad r_{\mathcal{D}}(a_{\mathcal{D}} = 1) \equiv 0, \quad (21)$$

where the expression for  $\kappa_{\mathcal{D}}$  (15) has been used.<sup>f</sup>

### 3. Methods

We use the Joint Light-curve Analysis (JLA) sample<sup>20</sup> containing 740 supernovae to test the scaling solutions described in Sec. 2. The JLA catalogue gathers data from four independent studies: SuperNovae Legacy Survey (SNLS), Sloan Digital Sky Survey (SDSS), nearby supernovae (Low- $z$ ), and Hubble Space Telescope (HST).

<sup>e</sup>We henceforth drop the domain index for the redshift.

<sup>f</sup>The expression (21) for  $dr_{\mathcal{D}}/da_{\mathcal{D}}$  is different from that in Eq. (41) of Ref. 17, which is due to minor typos in Ref. 17; see also the remarks in Ref. 18.



### 3.1. The SALT2 method

The Spectral Adaptive Lightcurve Template 2 (SALT2) method for making supernovae standard candles consists in fitting the supernovae light-curves to an empirical template, and subsequently using the parameters of the light-curve fit in the empirical model for band correction:

$$\mu_{SN} = m_B^* - M_B + \alpha x_1 - \beta c, \quad (22)$$

where  $m_B^*$  is the peak of the apparent magnitude in the B-band,  $M_B$  is the intrinsic magnitude in the rest frame of the supernova,  $x_1$  is the light-curve stretch parameter, and  $c$  is the colour correction parameter for each supernova in the sample.  $m_B^*$ ,  $x_1$ , and  $c$  are obtained from template fitting of the supernovae light-curves;<sup>20</sup>  $\alpha$  and  $\beta$  are global regression parameters that are determined in the fit.

### 3.2. The Likelihood function

We now briefly review the likelihood function  $\mathcal{L}(\hat{X} | \theta)$  used in this analysis, where  $\hat{X} = \{\hat{m}_{B,1}^*, \hat{x}_{1,1}, \hat{c}_1, \dots, \hat{m}_{B,N}^*, \hat{x}_{1,N}, \hat{c}_N\}$  are the ‘observed’ parameters for the supernovae labelled  $1, \dots, N$ , and  $\theta$  is short for all model assumptions (cosmological model, model for band correction, etc.).

The hats over the parameters in  $\hat{X}$  indicate that these parameters are inferred from data, whereas the corresponding parameters without hats represent the ‘true’ underlying (or intrinsic) parameters.

We use the likelihood function as formulated in Ref. 26, with the model for the distribution of intrinsic supernovae parameters proposed in Ref. 27, where the intrinsic parameters  $M_B, x_1, c$  of each supernova are assumed to be drawn from identical and independent Gaussian distributions with means  $M_0, x_{1,0}, c_0$  and standard deviations  $\sigma_{M_0}, \sigma_{x_{1,0}}, \sigma_{c_0}$ . Using the SALT2 relation (22) and the assumptions presented in Ref. 27, the final expression of the likelihood function is

$$\begin{aligned} \mathcal{L} = & |2\pi (\Sigma_d + A^T \Sigma_1 A)|^{-1/2} \\ & \times \exp \left[ -(\hat{Z} - Y_0 A) (\Sigma_d + A^T \Sigma_1 A)^{-1} (\hat{Z} - Y_0 A)^T / 2 \right], \end{aligned} \quad (23)$$

where  $|\cdot|$  denotes the determinant of a matrix,  $\Sigma_d$  is the estimated experimental covariance matrix (including statistical and systematic errors), and  $\Sigma_1$  is the ‘intrinsic covariance matrix’  $\text{diag}(\sigma_{M_0}^2, \sigma_{x_{1,0}}^2, \sigma_{c_0}^2, \sigma_{M_0}^2, \sigma_{x_{1,0}}^2, \sigma_{c_0}^2, \dots)$  of dimension  $3N \times 3N$ ;  $\hat{Z} \equiv \{\hat{m}_{B,1}^* - \mu_1, \hat{x}_{1,1}, \hat{c}_1, \dots, \hat{m}_{B,N}^* - \mu_1, \hat{x}_{1,N}, \hat{c}_N\}$ , where  $\mu_1, \dots, \mu_N$  are the distance moduli evaluated at the measured redshifts  $\hat{z}_1, \dots, \hat{z}_N$  of the supernovae, and  $Y_0 \equiv \{M_0, x_{1,0}, c_0, M_0, x_{1,0}, c_0, \dots\}$ ;  $A$  is the block diagonal matrix

$$A = \begin{pmatrix} 1 & 0 & 0 & 0 \\ -\alpha & 1 & 0 & 0 \\ \beta & 0 & 1 & 0 \\ 0 & 0 & 0 & \ddots \end{pmatrix}. \quad (24)$$

10 CÉLIA DESGRANGE, ASTA HEINESEN AND THOMAS BUCHERT

The final likelihood thus contains the following eight free parameters:  $\alpha$ ,  $\beta$ ,  $M_0$ ,  $x_{1,0}$ ,  $c_0$ ,  $\sigma_{M_0}$ ,  $\sigma_{x_{1,0}}$ , and  $\sigma_{c_0}$  in addition to the cosmological parameters entering the expression for the distance modulus  $\mu$ .

It has been suggested to include even more empirical parameters in order to model redshift-dependence in the intrinsic supernovae parameters and observational biases in these.<sup>28g</sup> In this paper we stick to the minimal likelihood model presented.

#### 4. Data analysis

We now constrain the parameter space of the scaling solutions with the JLA catalogue using the SALT2 relation and the likelihood model specified in Sec. 3.2. We then compare the quality of fit to that of the spatially flat  $\Lambda$ CDM model, the Milne universe model with no sources and a negative constant curvature (henceforth named the ‘empty universe model’), and the timescape model. We discuss the scales of application of the scaling solutions in relation to the application of a redshift-cut in the data in Sec. 4.1. In Sec. 4.2 we present our results.

##### 4.1. Statistical homogeneity scale and cut-off in redshift

Any model describing light propagation on a given scale should, for the sake of self-consistency, only be applied to light-rays propagating over at least that scale.

Since all the models tested in this analysis have, per construction, structureless geometry and are designed to hold above an approximate statistical homogeneity scale, it is natural (or even mandatory) to impose a cut-off in radius relative to the observer corresponding to the approximate homogeneity scale. Light emitted by supernovae below such a radius is probing scales below which the cosmological averaged metric description applies.

The largest scales of second-order correlations between structures (applying a cut-off of  $\sim 1\%$  in the two-point correlation function)<sup>30</sup> is estimated to be  $\sim 70-120$  Mpc/h in  $\Lambda$ CDM.<sup>h</sup> Following Ref. 29 we apply a cut-off at a redshift radius in the CMB frame  $z_{\text{CMB,min}} = 0.033$  relative to a central observer, corresponding to a comoving distance of  $\sim 100$  Mpc/h. This choice is a bit more conservative than that imposed in Ref. 32 of  $z_{\text{CMB,min}} = 0.024$ . The slight difference in choice of cut-off does not strongly affect the final results.

##### 4.2. Results

We use the likelihood function given in Sec. 3.2 and the equation for the distance modulus (16) to constrain the scaling solutions.

<sup>g</sup>For a discussion on the degeneracy introduced between parameters that describe the supernovae and the cosmological model in such empirical modeling, see Ref. 29.

<sup>h</sup>Note that higher-order correlations are still significant on Gpc scales. Probed through Minkowski functionals containing all orders of correlation functions, the analysis of SDSS LRG samples revealed more than  $2\sigma$  deviations from  $\Lambda$ CDM mock catalogues on scales beyond 600 Mpc/h.<sup>31</sup>

The best-fit results are shown in Table 1, together with the corresponding results for the spatially flat  $\Lambda$ CDM model, the empty universe model, and the timescape model (see Table 2 of Ref. 29). It should be noted that the matter cosmological parameters  $\Omega_m^{\mathcal{D}_0}$  of all the models cannot be directly compared (even though they are represented by the same symbol to ease the notation). The scaling solutions, the spatially flat  $\Lambda$ CDM model, and the timescape model are non-nested (i.e. none of the models can be obtained from any of the other models by parameter space constraints), and their expansion history depend on  $\Omega_m^{\mathcal{D}_0}$  in different ways.

Table 1: Best-fit parameters and 68% confidence bounds.

Model	Scaling solution	$\Lambda$ CDM	Empty Universe	Timescape
$n$	$-1.1^{+0.1(1\sigma)}_{-0.2(1\sigma)}$	-	-	-
$\Omega_m^{\mathcal{D}_0}$ or $\Omega_{m_0}$	$0.24^{+0.04(1\sigma)}_{-0.04(1\sigma)}$	$0.37^{+0.03(1\sigma)}_{-0.03(1\sigma)}$	0	$0.31^{+0.07(1\sigma)}_{-0.09(1\sigma)}$
$\alpha$	0.13	0.13	0.13	0.13
$x_{1,0}$	0.11	0.11	0.10	0.11
$\sigma_{x_{1,0}}$	0.90	0.90	0.90	0.90
$\beta$	3.1	3.1	3.1	3.1
$c_0$	-0.021	-0.022	-0.020	-0.021
$\sigma_{c_0}$	0.069	0.069	0.069	0.069
$M_{B,0}$	-19	-19	-19	-19
$\sigma_{M_{B,0}}$	0.10	0.10	0.11	0.10

The frequentist  $1\sigma$  and  $2\sigma$  confidence contours for the scaling solutions are shown in Fig. 1. Our results are consistent with positive present-epoch volume acceleration, ruling out deceleration at the  $> 2\sigma$  level, for the class of scaling solutions tested.

A striking result is that the best-fit scaling index  $n = -1.1^{+0.1(1\sigma)}_{-0.2(1\sigma)}$  is consistent with the results obtained in Ref. 33 in a perturbative framework around an Einstein-de Sitter background, where the leading-order (or largest-scale) backreaction was found to obey the scaling law  $\mathcal{Q}_{\mathcal{D}} \propto a_{\text{EdS}}^{-1}$ . The best-fit scaling index is thus compatible with a perturbative evaluation of backreaction (extrapolating the perturbative scaling law). Notice also that the best-fit scaling index is significantly different from the case of a scaling solution  $n = 0$  mimicking a cosmological constant, *cf.* Ref. 23 [Sect. 3.3.2].

Comparing Fig. 1 with the contour plot of Ref. 17 based on CMB data from WMAP3-yr data and 71 SNIa from the SNLS Collaboration, there is a significant amount of overlap of the  $2\sigma$  contours. However, the volume of the likelihood in the present analysis is shifted towards lower values of  $\Omega_m^{\mathcal{D}_0}$  and  $n$  as compared to

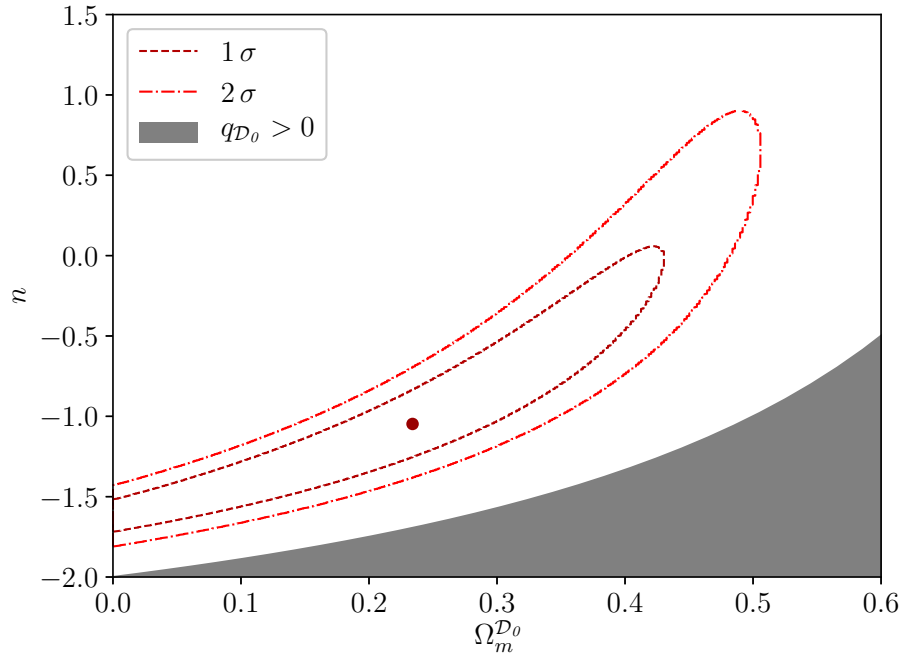


Figure 1:  $1\sigma$  and  $2\sigma$  confidence contours of the parameters  $\Omega_m^{D_0}$  and  $n$  of the scaling solutions. The best-fit,  $\{\Omega_m^{D_0} = 0.24, n = -1.1\}$ , is marked by a dot. The shaded area represents models with present-epoch volume deceleration  $q_{D_0} > 0$ , and the remaining area of the parameter space has positive present-epoch volume acceleration. Thus, deceleration is ruled out at the  $> 2\sigma$  level for the class of scaling solutions tested.

Ref. 17.<sup>i</sup>

Comparing with the constraints on the scaling solutions from Ref. 18, obtained from measurements of the Hubble parameter from the differential age method and radial baryon acoustic oscillation data, we find agreement within  $1\sigma$  of the scaling index  $n$  and a marginal tension of  $\sim 2\sigma$  for the matter cosmological parameter  $\Omega_m^{D_0}$ .

We compare the quality of fit of the scaling solutions with that of the spatially  $\Lambda$ CDM model, the empty universe model, and the timescape model using the *Akaike Information Criterion* (AIC).<sup>34</sup> The AIC is a measure of the relative probability of

<sup>i</sup>It is difficult to compare with the results of Ref. 17 because of the sparse supernova sample used and since the best-fit is obtained from a combination of the supernova and CMB data. Moreover, the error-bars on the best-fit parameters are not quoted. Generally, we refer to Ref. 17 with respect to the theoretical foundations and methods, the results obtained therein are by now outdated.

minimal information loss between two models:

$$\frac{p_1}{p_2} = \frac{\exp(-AIC_1/2)}{\exp(-AIC_2/2)}; \quad AIC_i \equiv 2q_i - 2\ln(\mathcal{L}_i), \quad (25)$$

where  $q_i$  is the number of parameters and  $\mathcal{L}_i$  is the maximum likelihood of model  $i$ , where  $p_i$  is the probability that model  $i$  minimizes the (estimated) information loss, and where the two models are labelled  $i = 1, 2$ , respectively. The AIC relative likelihood measure (25) can be viewed as a generalization of the likelihood ratio to non-nested models.

We show the results of the AIC relative likelihood measure in Table 2. We use the spatially flat  $\Lambda$ CDM model as reference, and quote  $p_{\text{model}}/p_{\Lambda\text{CDM}}$  for a given model. In addition to the scaling solution with two free cosmological parameters,  $n$  and  $\Omega_m^{\mathcal{D}_0}$ , the AIC is also computed for the constrained scaling solution with the scaling index fixed to its large-scale theoretical expectation from Lagrangian perturbation theory studies<sup>33</sup>  $n = -1$ .

Table 2: Number of parameters, AIC, and the AIC relative likelihood. The AIC relative likelihood is shown with the  $\Lambda$ CDM model as reference.

Models	Scaling solution	Scaling solution <sup><math>n=-1</math></sup>	$\Lambda$ CDM	Empty Universe	Timescape
Number of parameters	10	9	9	8	9
AIC	-225	-227	-227	-222	-227
$p_{\text{model}}/p_{\Lambda\text{CDM}}$	0.4	1.0	1.0	0.1	1.0

We infer from Table 2 that the relative probability of minimal information loss is close between the models, which differ at most by a factor of 10 in AIC likelihoods. The AIC likelihoods of the scaling solutions, the  $\Lambda$ CDM model, and the timescape model are well within one order of magnitude of each other. The AIC likelihood for the constrained scaling solution with  $n = -1$  is slightly higher than for the unconstrained case. This is because the best-fit scaling index for the unconstrained scaling solution is close to  $n = -1$ , and thus the expense of the additional parameter is not outweighed by an increase in likelihood.

We note that the slight disfavouring of the empty universe model relative to the other models is not robust to subsampling of data. E.g. if we implement a redshift cut of  $z_{\text{CMB,min}} = 0.07$  (leaving 613 SNIa in the sample), the AIC relative likelihood of the empty universe model versus  $\Lambda$ CDM increases to 0.4. We conclude that all five models fit the data equally well.

Our findings align with the conclusions in the recent investigation of the Pantheon sample in Ref. 35 in which it is found that data is little constraining for  $z > \sim 1$ , allowing for possibly large deviations from  $\Lambda$ CDM, and with the results of Ref. 27 reporting marginal evidence for acceleration within the FLRW framework.

We note that neither the scaling solutions, the timescape model, nor the empty universe model have any local energy-momentum component violating the strong energy condition.

### 5. Testing curvature dynamics with upcoming surveys

It is of observational interest to investigate possible signatures distinguishing between models with dynamical spatial curvature and FLRW models (with rigid spatial curvature).

To test the FLRW constant spatial curvature hypothesis, we can note that minus the spatial curvature density parameter  $\Omega_{k_0}$  of FLRW cosmology can be written:<sup>36</sup>

$$k_H = \frac{1}{D^2} \left( 1 - \left( \frac{dD}{dz} \frac{H}{H_0} \right)^2 \right), \quad (26)$$

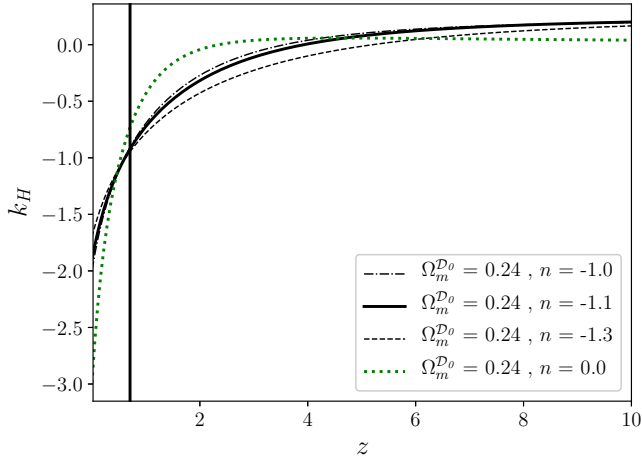
where  $D$  is the dimensionless FLRW comoving distance related to the angular diameter distance  $d_A$  by  $D = H_0/c(1+z)d_A$ , and where  $H$  is the FLRW Hubble parameter, and  $k_H = -\Omega_{k_0}$  per construction. For any other model with a prediction of angular diameter distance and volume expansion as a function of redshift, we might also construct the function  $k_H$  (26). In general,  $k_H$  is not interpreted as a spatial curvature density parameter, but simply as the combination of distance measures given by the right-hand side of (26), and it is in principle allowed to vary arbitrarily with redshift.

Computing  $r_{\mathcal{D}}$  and  $H_{\mathcal{D}}$  for the best-fit scaling solution,  $\{\Omega_m^{\mathcal{D}_0} = 0.24, n = -1.1\}$ , and substituting  $D = H_{\mathcal{D}_0}/c(1+z)d_A = H_{\mathcal{D}_0}/c\hat{k}^0 r_{\mathcal{D}}$  and  $H = H_{\mathcal{D}}$  in (26), we obtain  $k_H$  and  $d k_H/dz$  as a function of redshift as shown in Fig. 2. We also show the 68% confidence bounds on  $n$  while keeping  $\Omega_m^{\mathcal{D}_0}$  fixed (varying  $\Omega_m^{\mathcal{D}_0}$  within its 68% confidence bounds leave  $k_H$  and  $d k_H/dz$  almost unchanged). Note that the JLA sample contains supernovae at redshifts  $z \lesssim 1.3$ . We nevertheless show the prediction of  $k_H$  for higher redshifts.

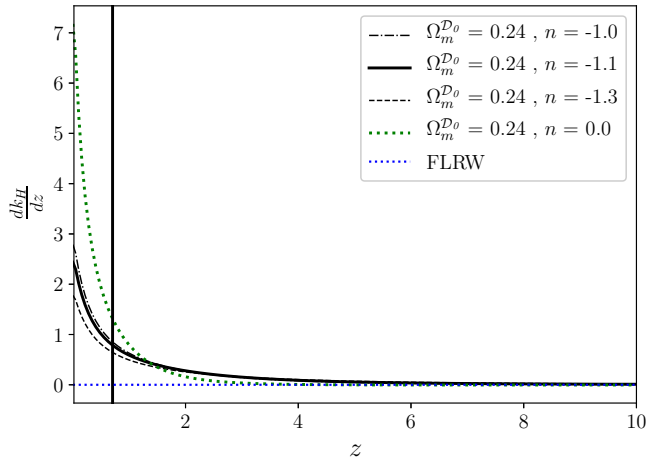
The evolution of  $k_H$  of the best-fit scaling solution is far from the constant- $k_H$  signature of an FLRW model. The effective curvature parameter  $k_H$  tends to increasingly negative values when approaching the present epoch  $z \rightarrow 0$ , and tends to a constant close to zero in the early universe limit.

The deceleration parameter (11) decreases with decreasing redshift and becomes negative at  $z \sim 0.7$  for the best-fit scaling solution,  $\{\Omega_m^{\mathcal{D}_0} = 0.24, n = -1.1\}$ , marking the transition between volume deceleration to volume acceleration in the best-fit model. This redshift of transition is comparable to that predicted by  $\Lambda$ CDM.

Interestingly, our results for the scaling solutions show tendencies similar to those of Ref. 37 (see their Fig. 6) where model-independent fitting functions are



(a) The function  $k_H$ , equation (26), predicted by the best-fit scaling solution found in this paper. For a FLRW model universe  $k_H = -\Omega_{k_0}$ , where  $\Omega_{k_0}$  is the spatial curvature density parameter evaluated at the present epoch.



(b)  $dk_H/dz$  as predicted by the best-fit scaling solution found in this paper. In a FLRW model universe  $dk_H/dz = -d\Omega_{k_0}/dz = 0$ .

Figure 2:  $k_H$  and  $dk_H/dz$  as a function of redshift for the best-fit scaling solution,  $\{\Omega_m^{D_0} = 0.24, n = -1.1\}$ . The scaling index upper and lower 68% confidence bounds,  $n = -1.1_{-0.2}^{+0.1}$ , are shown for fixed  $\Omega_m^{D_0}$ . The solution for  $\{\Omega_m^{D_0} = 0.24, n = 0\}$  is shown as well as a reference. The vertical grey line marks the redshift of transition from volume deceleration to volume acceleration as predicted by the best-fit model.

used to determine the best-fit shape of  $k_H$  from the JLA sample, SDSS-III BOSS BAO measurements, and differential age measurements of galaxies.

In the model-independent determination of  $k_H$  in Ref. 37, negative values of  $k_H$  are favoured towards lower redshifts as shown in their Fig. 6, consistent with our Fig. 2a. Despite of these best-fit tendencies in Ref. 37, the  $\Lambda$ CDM  $k_H = 0$  curvature constraint is still satisfied within the 95% confidence intervals of their analysis using present data.

We emphasize that the best-fit scaling index  $n = -1.1$  is obtained when assuming the model to be a single-scaling solution. More refined modeling of inhomogeneities, e.g. in terms of two-scale volume partitioning into overdense and underdense regions,<sup>38,39</sup> feature an additional effect due to the expansion variance between the two regions that adds volume acceleration, pushing the overall scaling index to values closer to 0. Although the distance modulus–redshift relation of multi-scale models is different, and thus these refined models cannot be directly compared with the single-scaling solution, we show the reference line  $n = 0$  in Fig. 2 to illustrate that even a drastic change in the scaling-index will not significantly change the observational prediction on deviations from a constant-curvature geometry. The transition from zero FLRW curvature signature  $k_H \sim 0$  to negative FLRW curvature signature  $k_H \lesssim -1$  is sharper in the  $n = 0$  case; it may therefore be easier to observationally distinguish this case from the constant  $k_H$  signature of a FLRW model.

With next generation data (such as upcoming surveys from LSST and Euclid<sup>‡</sup>) the predictions of Fig. 2 and complementary distance combinations will be useful for discriminating between the  $\Lambda$ CDM model, the scaling solutions, as well as other models with non-trivial curvature evolution.

## 6. Conclusion

We have investigated the fit of the scaling solutions, which are a class of solutions for the evolution of averaged cosmological variables, constrained by the exact average properties of Einstein’s equations and supplemented with a compatible but idealised template metric, to the Joint Light-curve Analysis (JLA) sample of 740 SNIa.

We find constraints that are roughly in agreement with previously found constraints based on SNIa, CMB, the differential age method, and baryon acoustic oscillation measurements in Ref. 17, 18, though we find a minor  $\sim 2\sigma$  tension when comparing to the matter cosmological parameter  $\Omega_m^{\mathcal{D}_0}$  quoted in Ref. 18.

Our result for the scaling index  $n$  is consistent with theoretical expectations on the large-scale behaviour of backreaction within an averaged Lagrangian perturbation approach, Ref. 33.

Comparing the fit of the scaling solutions, the  $\Lambda$ CDM model and the timescape

<sup>‡</sup>See Ref. 40 for performance forecasts for the Euclid satellite and for a discussion of testable alternative frameworks, hereunder backreaction models, to that of the  $\Lambda$ CDM model.



model, we find that the models are equally preferred from data from an Akaike Information Criterion (AIC) perspective. The empty universe model is slightly less preferred in our primary fit, however, this conclusion is not robust to the subsampling of data. This suggests that a broad variety of models of the recent epoch expansion history can match currently available supernovae data.

Backreaction models, exemplified by scaling solutions that match JLA data, predict a clear signature in terms of a particular FLRW curvature consistency measure if compared with the FLRW class of space-times. This indicates that one might be able to significantly discriminate between models with evolving curvature and models with constant-curvature geometry with upcoming surveys using this measure.

**Acknowledgements:** This work is part of a project that has received funding from the European Research Council (ERC) under the European Union’s Horizon 2020 research and innovation programme (grant agreement ERC advanced grant 740021–ARTHUS, PI: TB). CD would like to thank all colleagues at CRAL for the nice ambiance at work during the summer internship. AH is supported by an University of Canterbury doctoral scholarship, and acknowledges hospitality for visits to CRAL–ENS, Lyon, supported by Catalyst grant CSG–UOC1603 administered by the Royal Society of New Zealand. AH is grateful for the support given by the funds: ‘Torben og Alice Frimodts Fond’, ‘Knud Højgaards Fond’, and ‘Max Nørgaard og Hustru Magda Nørgaards Fond’.

## Bibliography

1. A. G. Riess, et al., *Astron. J.* **116** (1998) 1009, [astro-ph/9805201](#).
2. S. Perlmutter, et al., *Astrophys. J.* **517** (1999) 565, [astro-ph/9812133](#).
3. S. Perlmutter, et al., *Bulletin of the American Astronomical Society* Vol. **29** (1997) 1351, [astro-ph/9812473](#).
4. W. L. Freedman, *Nature Astron.* **1** (2017) 0169, [arXiv:1706.02739](#).
5. P. A. R. Ade, et al., *Astron. Astrophys.* **594** (2016) A24, [arXiv:1502.01597](#).
6. H. M. Bourboux, et al., *Astron. Astrophys.* **608** (2017) A130, [arXiv:1708.02225](#).
7. B. D. Fields, *Ann. Rev. Nucl. Part. Sci.* **61** (2011) 47, [arXiv:1203.3551](#).
8. H. Hildebrandt, et al., *Mon. Not. Roy. Astron. Soc.* **465** (2017) 1454, [arXiv:1606.05338](#).
9. J. D. Bowman, A. E. E. Rogers, R. A. Monsalve, T. J. Mozdzen and N. Mahesh, *Nature* **555** (2018) 67.
10. C. L. Steinhardt, P. Capak, D. Masters and J. S. Speagle, *Astrophys. J.* **824** (2016) 21.
11. R. K. Sheth and A. Diaferio, *Mon. Not. Roy. Astron. Soc.* **417** (2011) 2938, [arXiv:1105.3378](#).
12. T. Buchert, A. A. Coley, H. Kleinert, B. F. Roukema and D. L. Wiltshire, *Int. J. Mod. Phys. D* **25** (2016) 1630007, [arXiv:1512.03313](#).
13. T. Buchert, *Gen. Relativ. Gravit.* **32** (2000) 105, [gr-qc/9906015](#).
14. T. Buchert, *Gen. Relativ. Gravit.* **33** (2001) 1381, [gr-qc/0102049](#).
15. X. Roy, T. Buchert, S. Carloni and N. Obadia, *Class. Quantum Grav.* **28** (2011) 165004, [arXiv:1103.1146](#).
16. T. Buchert, J. Larena and J.-M. Alimi, *Class. Quantum Grav.* **23** (2006) 6379, [gr-qc/0606020](#).

18 CÉLIA DESGRANGE, ASTA HEINESEN AND THOMAS BUCHERT

17. J. Larena, J.-M. Alimi, T. Buchert, M. Kunz and P.-S. Corasaniti, *Phys. Rev. D.* **79** (2009) 083011, [arXiv:0808.1161](#).
18. S.-L. Cao, H.-Y. Teng, H.-Y. Wan, H.-R. Yu and T.-J. Zhang, *EPJ C* **78** (2018) 170, [arXiv:1704.01774](#).
19. D. L. Wiltshire, *Phys. Rev. D.* **80** (2009) 123512, [arXiv:0909.0749](#).
20. M. Betoule, et al., *Astron. Astrophys.* **568** (2014) A22, [arXiv:1401.4064](#).
21. T. Buchert and M. Carfora, *Class. Quantum Grav.* **25** (2008) 195001, [arXiv:0803.1401](#).
22. M. Kasai, *Prog. Theor. Phys.* **117** (2007) 1067, [astro-ph/0703298](#).
23. T. Buchert, *Gen. Relativ. Gravit.* **40** (2008) 467, [arXiv:0707.2153](#).
24. P. C. Stichel, *Phys. Rev. D* **98** (2018) 104022, [arXiv:1805.08459](#).
25. N. Uzun (2018) [arXiv:1811.10917](#).
26. M. C. March, R. Trotta, P. Berkes, G. D. Starkman and P. M. Vaudrevange, *Mon. Not. Roy. Astron. Soc.* **418** (2011) 2308, [arXiv:1102.3237](#).
27. J. T. Nielsen, A. Guffanti and S. Sarkar, *Sci. Rep.* **6** (2016) 35596, [arXiv:1506.01354](#).
28. D. Rubin and B. Hayden, *Astrophys. J.* **833** (2016) L30, [arXiv:1610.08972](#).
29. L. H. Dam, A. Heinesen and D. L. Wiltshire, *Mon. Not. Roy. Astron. Soc.* **472** (2017) 835, [arXiv:1706.07236](#).
30. M. Scrimgeour, et al., *Mon. Not. Roy. Astron. Soc.* **425** (2012) 116, [arXiv:1205.6812](#).
31. A. Wiegand, T. Buchert and M. Ostermann, *Mon. Not. Roy. Astron. Soc.* **443** (2014) 241, [arXiv:1311.3661](#).
32. A. G. Riess, et al., *Astrophys. J.* **659** (2007) 98, [astro-ph/0611572](#).
33. T. Buchert, C. Nayet and A. Wiegand, *Phys. Rev. D.* **87** (2013) 123503, [arXiv:1303.6193](#).
34. H. Akaike, *IEEE Trans. Automat. Contr.* **19** (1974) 716.
35. B. L'Huillier, A. Shafieloo, E. V. Linder and A. G. Kim (2018) [arXiv:1812.03623](#).
36. C. Clarkson, B. Bassett, and T. H. Lu *Phys. Rev. Lett.* **101** (2008) 011301, [arXiv:0712.3457](#).
37. F. Montanari and S. Räsänen *J. Cosmol. Astropart. Phys.* JCAP **11** (2017) 032, [arXiv:1709.06022](#).
38. A. Wiegand and T. Buchert, *Phys. Rev. D* **82** (2010) 023523, [arXiv:1002.3912](#).
39. S. Krastanov: Constraints from Observations on Backreaction Models, *Master thesis M1, École Normale Supérieure de Lyon* (2012).
40. L. Amendola, et al. *Living Rev. Rel.* **21** (2018) 1, [arXiv:1606.00180](#).